Materials Advances

ROYAL SOCIETY OF CHEMISTRY

PAPER

View Article Online
View Journal | View Issue

Cite this: *Mater. Adv.*, 2023, 4, 6304

Highly conductive three-dimensional metal organic frameworks from small *in situ* generated ligands†

Uddit Narayan Hazarika,[a] Jhorna Borah,[a] Arobinda Kakoti,[a] Rinki Brahma,[b] Kangkan Sarmah,[c] Ankur Kanti Guha [c] and Prithiviraj Khakhlary *[a]

Four isostructural formate based electrically conductive metal organic frameworks namely, $[H_2N(CH_3)_2][M(HCO_2)_3]$ (M = Mn; **Mn-F**, M = Co; **Co-F**, M = Ni; **Ni-F**, and M = Zn; **Zn-F**), were synthesized with simple and cost effective methods. The *in situ* generated formate ion was attributed to decomposition of DMF, which was used as the solvent of the reactions, under high pressure and temperature conditions. Single crystal X-ray diffraction analysis reveals that MOFs also contain *in-situ* generated dimethyl ammonium cations inside their pores to maintain the charge neutrality of the framework. The as-synthesized MOFs exhibit impressive room temperature electrical conductivity compared to the MOFs reported so far. The conductivity is attributed to the charge (*in situ* generated) flow along the pores of the MOFs and electron flow through the metal–ligand bond owing to the metal d-orbital and ligand p-orbital overlap. All the MOFs are semiconducting in nature and their conductivities increase with temperature. **Mn-F** exhibits conductivity as high as 47.846 S cm^{-1} at 50 °C which was the highest among the conductivities of the four reported MOFs. Upon removal of guests from the pores the room temperature electrical conductivity of all the frameworks was improved except for **Co-F**. The formation of highly mobile hydronium ions upon removal of guests may be one of the reasons for improvement in the conductivity of the aforementioned de-guested MOFs. By the theoretical evaluation of the bonds of the MOFs, through bond conductivity is significantly determined by the number of high spin electrons in the metal d-orbitals.

Received 18th August 2023,
Accepted 21st October 2023

DOI: 10.1039/d3ma00562c

rsc.li/materials-advances

Introduction

During the past few years, research on metal organic frameworks (MOFs) has been tremendous as researchers use metal–organic frameworks as next-generation functional materials for a wide range of applications.[1,2] Metal organic frameworks comprise metal ions and organic ligands, and the latter allow synthetic as well as structural tunability leading to a wide range of physical properties. These physical properties have gained much attention because of their potential applications in gas storage, separation, catalysis *etc.*[3] However, MOFs are porous in nature with high surface area, and highly crystalline materials exhibit poor electrical conductivity or high charge mobility limiting their use in the fields of batteries, supercapacitors, electrocatalysis and sensing.[4] Therefore, recently significant efforts were made to improve the electrical conductivity properties of MOFs applying various strategies such as through-bond charge transport,[5] through-space charge transport,[1] in-plane π-conjugation,[6,7] and doping.[4,8,9] It is observed that formation of effective charge movement pathways plays a vital role in enhancing the conductivity properties of MOFs. Specially, active d-electron transition metals which have a suitable radius to achieve a better orbital overlap with the coordinating atom of the ligands are conductive with a small band gap and high charge mobility.[10] So, judicious selection of metal cations and coordinating atoms is very important for achieving good charge transport in MOFs.[5] Besides coordinating atoms, organic cores also have an important role in endowing MOFs with conductivity.[6] As for instance, conjugation of the organic part plays an important role in enhancing the electrical conductivity of MOFs through electron delocalization. As reported earlier metal–organic frameworks with highly conjugated ligand cores show high electrical conductivity.[11]

The formate anion, the smallest carboxylate ligand with a variety of bridging modes, can bind with 3d and 4f metals to form complexes in different coordination styles and some of

[a] *Department of Chemistry, Dibrugarh University, Dibrugarh, 786004, India. E-mail: pkhakhlary@dibru.ac.in*
[b] *Department of Chemistry, Indian Institute of Technology, Guawahati, 781039, India*
[c] *Department of Chemistry, Cotton University, Guwahati, Assam, 781001, India*

† Electronic supplementary information (ESI) available. CCDC 2263898, 2263916 and 2263917. For ESI and crystallographic data in CIF or other electronic format see DOI: https://doi.org/10.1039/d3ma00562c

these complexes also exhibit excellent magnetic properties.[12] Moreover, due to the charge delocalisation path in the formate anion analogous to other aromatic carboxylate ligands, such as DSBDC, DOBDC *etc.*,[3,4] the formate anion based MOFs are anticipated to exhibit charge mobility or electrical conductivity. With this anticipation, we envisaged electrically conductive MOFs based on formate anions. Therefore, herein we prepared a series of formate based electrically conductive MOFs using 3d transition metal cations (namely Mn^{2+}, Co^{2+}, Ni^{2+} and Zn^{2+}) and *in situ* generated formate anions from decomposition of DMF. The isostructural formate based MOFs of manganese, cobalt, nickel and zinc namely **Mn-F**, **Co-F**, **Ni-F** and **Zn-F**, respectively, exhibit significant electrical conductivity which increases with the increase of temperature indicating the semiconducting nature of these MOFs. The lattice structure of the MOFs contains *in situ* generated guest molecules. The removal of the guest molecules from the pores of the MOFs improved the conductivities of the MOFs, except one. Improvement in conductivity of the MOFs upon removal of guests is attributed to the generation of mobile hydronium ions as well as an increase in the number of high spin electrons of the d-orbital.

So far, most of the reports on conductive MOFs talk about designing highly conjugated ligands or 1D, 2D highly charged delocalized systems (MOFs) to achieve conductivity. In most of the cases, to achieve so, expensive reagents and some tedious experiments are involved. Again upon comparison with the previously reported electrically conductive MOFs significant advantages of the series of MOFs reported in this article were observed. As for instance, the ligands of the MOFs are generated *in situ* from the solvent used for the reaction, so no additional synthesis of an organic ligand is needed. MOFs were easier to synthesise as simply a saturated solution of a metal salt in DMF is enough to obtain MOFs, which is cost-effective in terms of no requirement of additional reagents for the reaction. The synthetic strategy is reproducible and highly crystalline MOFs may be produced in bulk. Again, obtained crystals enabled single crystal X-ray structural determination which is rare in the previous reports on conducting MOFs. Again, the conductivities of these MOFs are superior to those of many of the previously reported conductive MOFs. Therefore, this report offers a new avenue for development of economical and conductive MOFs and also conductive MOFs from small ligands. This work also discusses potential application of these MOFs in energy storage and provides insight of the structure–property relationship of conductive MOFs.

Results and discussion

From the reaction between metal salts (metals: Mn, Co, Ni and Zn) and DMF under solvothermal conditions, crystalline isostructural formate complexes of manganese, cobalt, nickel and zinc namely **Mn-F**, **Co-F**, **Ni-F** and **Zn-F** were obtained. Although the structures of these MOFs were previously reported,[13–16] in this work they were obtained from different synthetic methods. The structures of **Mn-F**, **Co-F**, **Zn-F** and **Ni-F** were resolved with the help of both single and powder XRD and compared with the reported data. Single crystal XRD structures were reported by various research groups. However, information regarding the physical appearance (size, shape, colour, crystallinity *etc.*) of crystals is rare. In Fig. 1 it can be observed that high quality crystals with significant size were obtained for four metal ions using our methods. Except for **Zn-F**, block shaped single crystals with various sizes were obtained for the rest of the MOFs. In the case of **Co-F**, the single crystal size is even up to 4 mm.[3] We have also tried to synthesize MOFs for metal ions such as iron and copper, however we could not get crystals from these systems. Rapid fluctuation of the oxidation states of these metal ions may be one of the reasons for not getting crystals using the present synthetic strategy. The *in situ* generated formate ion is attributed to the decomposition of DMF under high pressure and temperature conditions. Literature reports suggest that *N*,*N*-dimethyl formamide (DMF) molecules hydrolyse at high temperature and the rate of the reaction increases under acidic or basic conditions.[13] It was found that fine single crystals of **Mn-F** were only obtained upon addition of acid whereas **Co-F**, **Ni-F** and **Zn-F** were obtained without addition of acid. It may be due to the fact that in the latter cases the inherent acidity of metal ions was enough to proceed the hydrolysis reaction while in the former, less acidic manganese ions require additional acid to hydrolyse *N*,*N*-dimethylformamide at 120 °C.

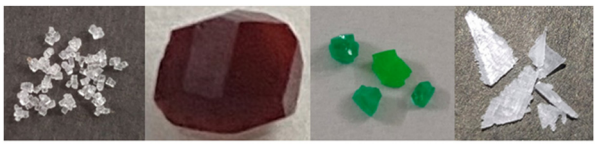

Fig. 1 Images of crystals of MOFs.

All the MOFs crystallise in the trigonal unit cell with an $R\bar{3}c$ space group. The metal ions are in octahedral geometry to build a 3-dimensional coordination polymer. Formate ions act as a bridging ligand with μ_2 type binding mode to connect two metal ions at a time (Fig. 2a). In each case the formate ion binds to the metal centres in *anti–anti* mode. The C–O bond length is between single and double bond which suggests a partial double bond between the two atoms. As the previous reports suggest the asymmetric unit contains three formate anions, one M^{2+} metal cation and to balance the charge one *in situ* generated dimethyl ammonium cation. The dimethyl ammonium cation resides into the pores of the MOF crystal lattice (Fig. 2b). Removal of the guest molecules from the pores can make the MOFs significantly porous (Fig. 2c). In all the cases, the axial positions of the octahedra are in the opposite direction owing to the *anti-anti* mode of bridging of the formate anion (Fig. 2d). Since the dimethyl ammonium cation (DMA) is associated with all the crystal structures it clearly indicates that DMA plays a crucial role in the formation of the 3D networks. The DMA cation was found to be significantly disordered in nature and consequently increases the residual peaks of the structure.

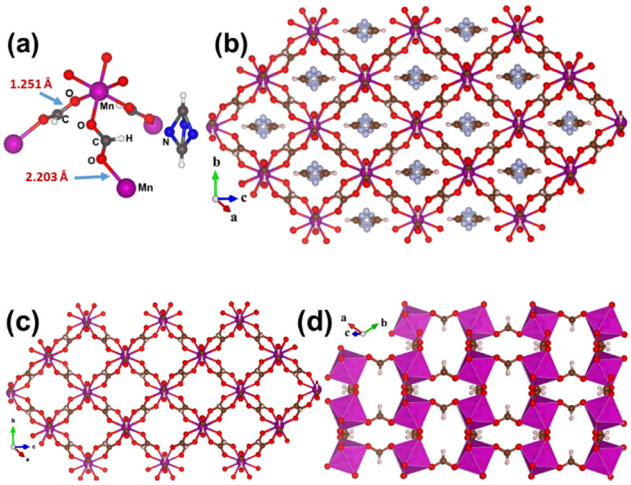

Fig. 2 (a) Asymmetric unit of **Mn-F**; structure of **Mn-F** (b) with and (c) without entrapped guest molecules (DMA); and (d) coordination polyhedra of **Mn-F**.

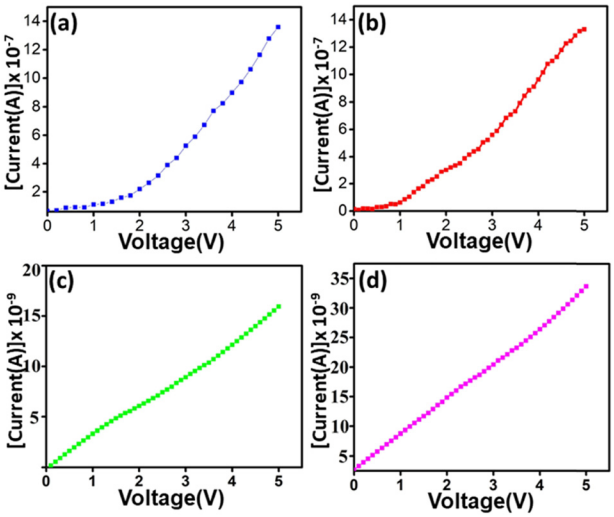

Fig. 4 *I–V* curves of (a) **Mn-F**, (b) **Co-F**, (c) **Ni-F** and (d) **Zn-F** MOFs recorded at 30 °C.

Since the formate ion has delocalized electrons and the frameworks contain $(–M–O–)_\infty$ chains, we anticipated electrical conductivity in the MOFs through the M–O bonds. Again, the MOFs contain charged guest molecules which can significantly contribute to the proton conductivity. The current with respect to applied voltage was recorded using a source meter (Keithley 2400) and subsequently electrical conductivity of the MOFs at room temperature was determined. To do so the crystals of each of the MOFs were finely ground to powder and suitable pellets were prepared with the help of a hydraulic press by applying a pressure of *ca.* 2–5 ton. To measure the conductivities, the pellets so obtained were placed between a probe and a copper strip connected to another probe in a two probe sample holder as shown in Fig. 3.

The *I–V* curves of all the four MOFs were determined at room temperature (*ca.* 30 °C) and at 60% humidity. In all the cases current shows a linear response to applied potential indicating that the MOFs are ohmic materials (Fig. 4). From the *I–V* curves corresponding conductivity of the respective MOFs was determined (Table 1). All the MOFs exhibited impressive electrical conductivity compared to the majority of the conductive MOFs reported so far and some of the reported conductivities of MOFs are listed in Table S1 (ESI†).

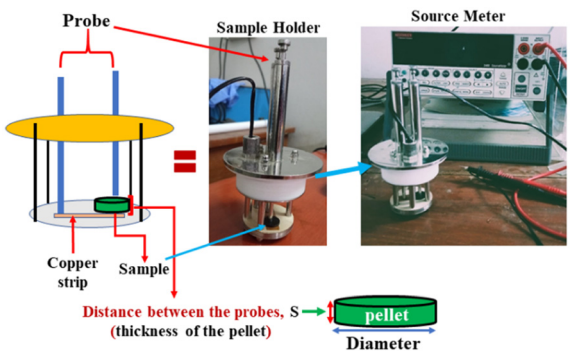

Fig. 3 Conductivity measurement set up.

As mentioned, conductivity of the MOFs may be due to (1) proton conductivity owing to the presence of the $(CH_3)_2NH_2$ cation and (2) electrical conduction due to through bond electron flow between the metal ion and the ligand.[10] Among the as-synthesized MOFs, **Mn-F** has the highest conductivity as it has the highest pore volume (predicted from M–O and C–O bond lengths) which facilitates easy movement of the guest molecules to conduct electricity. As we go from **Mn-F** to **Zn-F** conductivity decreased which may be attributed to a decrease in pore sizes as one of the reasons as the M–O and C–O bond shortened (Fig. S2 and S3, ESI†).

Moreover, charge flow along the metal–ligand bond may be expected to be the highest in **Mn-F** due to the fact that electronegativity of a metal ion is inversely related to the through bond conductivity.[17] Since the electronegativity order is $Mn^{2+} < Co^{2+} < Ni^{2+} < Zn^{2+}$, **Mn-F** will have the highest through bond conductivity value among the MOFs. Again, it may also be viewed that Mn^{2+} has the highest number of unpaired d-electrons compared to Co, Ni and Zn and it decreases from Mn^{2+} to Zn^{2+} accordingly. Thus, combining the contributions from proton conductivity and through bond conductivity we can expect the conductivities of these MOFs as listed in Table 1.

In order to understand the band structure and the extent of the contribution of through bond conductivity to overall conductivity of the MOFs the band gap and partial density of states

Table 1 Conductivities of the as-synthesized MOFs

MOFs	Conductivity (S cm^{-1})
Mn-F	4.237×10^{-1}
Co-F	3.015×10^{-1}
Ni-F	4.872×10^{-3}
Zn-F	4.785×10^{-3}

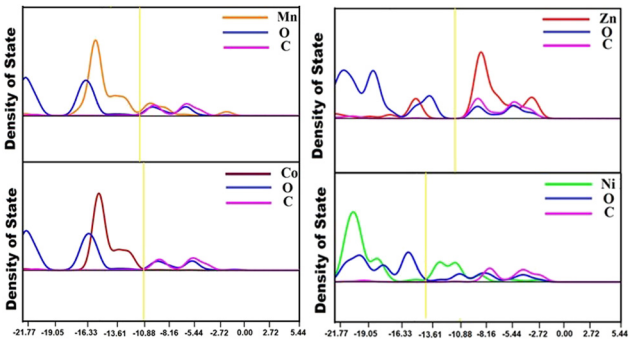

Fig. 5 PDOS curves for **Zn-F**, **Ni-F**, **Mn-F** and **Co-F** metal organic frameworks. The Fermi level is shown in a yellow vertical line.

(PDOS) were theoretically evaluated (Fig. 5). From the PDOS it is obvious that in the MOFs there is significant overlap between the metal d-orbital and the ligand p-orbital (the 2p orbital of oxygen atoms). Furthermore the DOS in all the cases are near to the Fermi level (yellow line) which indicates the semiconducting nature of the MOFs.

The electrical band gaps of the MOFs were determined theoretically. The band gaps range from 1.5 eV to 2.43 eV based on the type of the metal centre of the MOFs (Fig. S4, ESI†). It should be noted that these values are within the range of the band gaps of reported semiconductors. **Co-F** has the least band gap (1.53 eV) while **Zn-F** has the highest (2.43 eV), and **Mn-F** and **Ni-F** have band gaps of 1.97 eV and 2.0 eV, respectively. If looked carefully it may be observed that band gaps are governed by the extent of electron exchange between the metal centre and the ligand. It is obvious that Mn^{2+} ($3d^5$) and Zn^{2+} ($3d^{10}$) have half-filled and full-filled d-orbitals, respectively, which impart extra stability to these metal centres and minimize the electron exchange with the ligand and decrease the d-metal and p-ligand orbital overlap consequently increasing the band gap. However, in the cases of Ni^{2+} ($3d^8$) and Co^{2+} ($3d^7$), availability of unpaired d-orbitals may facilitate the ligand to metal electron flow which is expected to be the highest in the latter. Hence, the band gap may be expected to be the least in the case of the MOF containing the Co(II) centre followed by that containing the Ni(II) centre according to theoretical calculations.

From the theoretical investigation, it may be stated that the MOFs would exhibit significant electrical conductivity even in the absence of charged species inside the pores of MOFs.

Again, temperature dependence conductivity of the as-synthesized MOFs was studied by measuring the conductivity of the MOFs at different temperatures. The conductivity of the MOFs increases with an increase in temperature indicating the semiconducting nature of the MOFs (Fig. 6).

The increase in conductivities of the MOFs with temperature is obvious from the fact that the mobility of the guest molecules is enhanced as well as the electron flow through the metal–ligand bond may be facilitated with an increase of temperature.[18] The optimum temperature for the conductivity of MOFs is different for different types of metal centres. In the

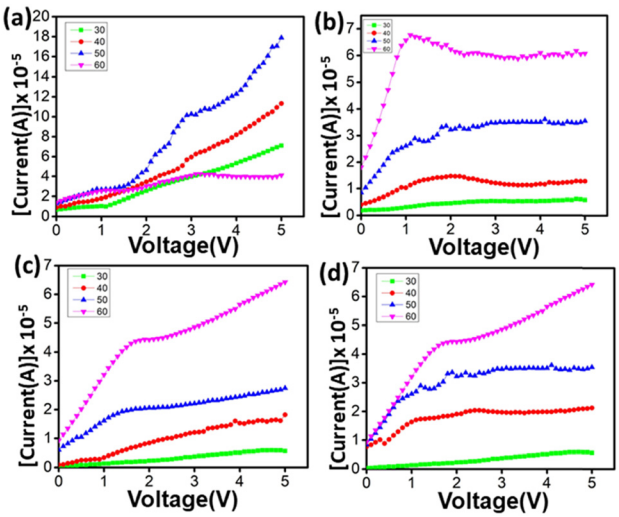

Fig. 6 Temperature dependent *I*–*V* curves of (a) **Mn-F**, (b) **Co-F,** (c) **Ni-F** and (d) **Zn-F** MOFs. Measured conductivities at different temperatures are represented with different colour lines: green line (30 °C), red line (40 °C), blue line (50 °C) and pink line (60 °C).

case of **Mn-F** conductivity increases up to 50 °C then decreases upon further increasing the temperature. However, in the cases of **Co-F**, **Ni-F** and **Zn-F** conductivity increases beyond 50 °C. The above observation may be understood from the fact that a larger pore volume in **Mn-F** may allow a significant increase in the thermal vibrations of the guest molecules which certainly contribute to induced resistance with temperature. Moreover, the Mn–O bond length is longer compared to the Co–O, Ni–O and Zn–O bond lengths which indicates higher thermal vibrations of the Mn–O bond compared to those of Co–O, Ni–O and Zn–O bonds at a given temperature. Moreover, the C–O bond length decreases on going from **Mn-F** to **Zn-F** as evident from the C–O bond stretching frequency in the respective MOFs (Table S2 and Fig. S5, ESI†). Aforementioned factors will significantly increase the resistance owing to the lattice vibrations of **Mn-F** consequently decreasing the conductivity after 50 °C unlike **Co-F**, **Ni-F** and **Zn-F**.

Comparing **Co-F**, **Ni-F** and **Zn-F,** it was observed that at a temperature of 60 °C and at higher voltage, in the case of **Co–F** current decreases with the increase of voltage while in **Ni-F** and **Zn-F** current increases with voltage, however upon increasing the current voltage decreases. This observation may be due to the fact that as the resistance of **Co-F** is higher than that of **Ni-F** and **Zn-F** as aforementioned, at higher voltage the induced temperature owing to resistance in **Co-F** is higher which further contributes to the resistance. Moreover, the Co–O bond is longer than Ni–O which clearly indicates higher thermal vibrations of the metal–O bond in **Co-F** at a given temperature. The highest conductivities achieved for each of the MOFs are given in Table 2. These conductivities are superior to those of many of the highly conjugated 1D and 2D conductive MOFs reported so far (Table S1, ESI†). One more aspect that makes these MOFs fascinating is they are 3D in nature which is rare in conductive MOFs.[19] From the changes in the conductivities of the MOFs

Table 2 Maximum conductivity of MOFs and the corresponding temperatures

MOFs	Conductivity (S cm^{-1})	Temperature (°C)
Mn-F	47.846	50
Co-F	21.231	60
Ni-F	31.847	60
Zn-F	15.923	60

Table 3 Activation energy of charge mobility of MOFs

MOFs	Activation energy, E_a (eV)
Mn-F	0.00731
Co-F	0.01305
Ni-F	0.01590
Zn-F	0.01599

with temperature (Fig. S6, ESI†), the activation energies of charge mobility of the respective MOFs were determined and tabulated in Table 3.

The TGA analysis suggests that the guest molecules start to leave the pores of the MOF (**Mn-F** taken as the representative case) at temperature around 170 °C (Fig. S7, ESI†) and the MOF starts to decompose after 360 °C.[20] Therefore, the guest molecules (dimethyl ammonium cations) were removed by heating the MOFs at 160 °C for 24 h to check the conduction of the MOFs in the absence of guests. The resulting MOFs devoid of guests were namely d-**Mn-F**, d-**Co-F**, d-**Ni-F** and d-**Zn-F**. Considering the possibilities of structural changes upon removal of guest molecules the PXRD patterns were compared before and after removal of guest molecules (Fig. S8 and S9, ESI†). The analysis of diffraction patterns upon removal of guest molecules from the pores indicated that the framework of **Co-F** was stable up to 200 °C. While **Mn-F** exhibited structural changes at the mentioned temperature which may due to the distortion of the pore shape and size owing to the generation of vacant sites in the MOF.[21,22] It is noteworthy to mention that the conductivities were improved in all the cases except d-**Co-F** upon removal of guest molecules (Table 4). The increase in the conductivity of MOFs upon removal of the guest molecules may be due to (1) probable changes in the number of unpaired d-electrons; upon removal of the DMA guest, there is a probability of charge imbalance within the framework. To maintain the charge neutrality of MOFs, there may be a change in the oxidation states (+ 2 to +3) of metal cations wherever favourable. This is unlikely for d-**Mn-F** and d-**Zn-F** because the extra-stability of half-filled and full-filled d-orbitals of Mn^{2+} and Zn^{2+} cations, respectively, would hold the same oxidation state. But, for d-**Co-F** and d-**Ni-F**, there is a high chance for the change of

Table 4 Conductivity (30 °C) of the MOFs after removal of guests

MOFs	Conductivity (S cm^{-1})
d-**Mn-F**	5.279×10^{-1}
d-**Co-F**	1.052×10^{-1}
d-**Ni-F**	4.975×10^{-1}
d-**Zn-F**	1.492×10^{-1}

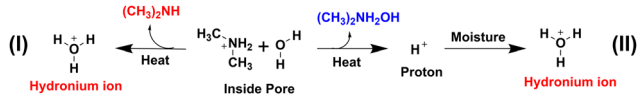

Scheme 1 Plausible reactions during heating to generate hydronium ions inside the pores of MOFs.

oxidation states. A change from high-spin to low-spin owing to the oxidation of Co^{2+} to Co^{3+} decreases the number of unpaired d-electrons which otherwise contributed to metal–ligand through bond conductivity. Unlike d-**Co-F**, for d-**Ni-F**, a change of Ni^{2+} to Ni^{3+} increases the number of unpaired d-electrons enhancing its through bond conductivity. Therefore, d-**Ni-F** will gain whereas d-**Co-F** will show through bond conductivity upon removal of the cationic guest. (2) The lattice vibration of the free $(CH_3)_2NH_2$ cation guest molecule may contribute to the vibration of the metal–ligand bond which may reduce the through bond conduction of the MOFs and (3) removal of guests from the pores results highly mobile protons to maintain the electrical neutrality of the resulting MOFs following one of the plausible paths given in Scheme 1.

It should be noted that the removal of cationic guests from the pores of the MOFs is only possible when the cationic guests transform into a neutral species during the heating. In the process a cationic species must be generated or a metal centre goes to a higher oxidation state to maintain the electroneutrality of the MOFs and to retain the basic framework of the MOFs. Since the framework of the MOFs was retained upon removal of the guest molecule as confirmed from PXRD analysis, we proposed the above reactions those generate cationic species inside the pores of the MOFs. Both the reactions finally generated hydronium ions which would maintain the electroneutrality and contribute to conductivity of the MOFs. Again, the change of the charge transport mechanism from vehicular to Grotthuss during the change from the DMA cation to the hydronium ion is expected to increase the proton conductivity.

From the above it is clear that all the deguested MOFs will gain conductivity owing to either an increase in the number of unpaired electrons or generation of highly mobile hydronium ions instead of bulky DMA cations. However, d-**Co-F** will lose conductivity due to the fact that the number of unpaired electrons decreases owing to the transformation of high spin Co^{2+} into low spin Co^{3+} during the removal of the guest. Again, in the meantime d-**Co-F** would also lose some of the hydronium ions which otherwise would have contributed to proton conductivity. To confirm this statement XPS analysis was performed before and after removal of guests for **Mn-F** and **Co-F** as representative cases (Fig. 7). The XPS 2p spectra of **Mn-F** exhibit a centre peak and a satellite peak with binding energies around 642.28 and 645 eV, respectively, which confirm the presence of only Mn^{2+} ions in the framework. Upon removal of guest molecules by heating no obvious change in the spectra was observed. While For **Co-F**, the centre peak was found at 780.46 eV with the shakeup satellite peak at 784.55 eV for $Co2p_{3/2}$, and for $Co2p_{\frac{1}{2}}$ the centre peak appeared at 796.27 eV with the shakeup satellite peak at 801.13 eV. Deconvolution of

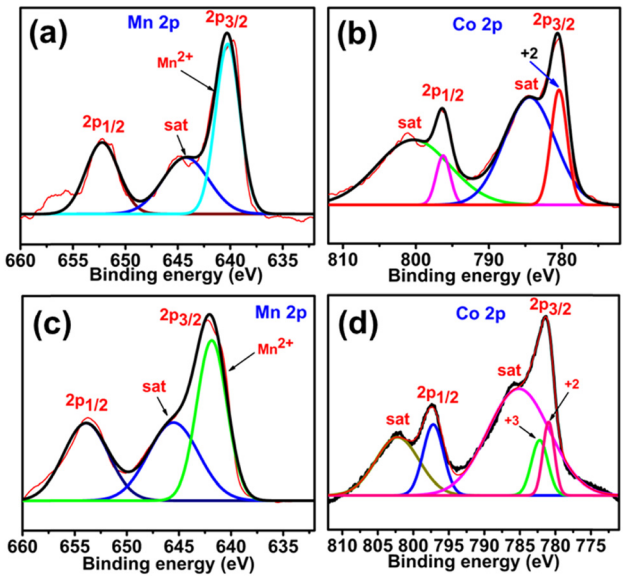

Fig. 7 XPS patterns of (a) **Mn-F**, (b) **Co-F**, (c) d-**Mn-F** and (d) d-**Co-F** MOFs.

$Co2p_{3/2}$ showed only one peak at 780.43 eV which corresponds to the Co^{2+} system. Unlike **Mn-F**, removal of guest molecules from **Co-F** induced oxidation of a fraction of the Co^{2+} centre. For $Co2p_{3/2}$, the centre peak was found at 781.43 eV with the shakeup satellite peak at 785.85 eV and for $Co2p_{\frac{1}{2}}$, the centre peak appears at 797.36 eV with the shakeup satellite peak at 802.32 eV. Deconvolution of $Co2p_{3/2}$ revealed two peaks at 780.94 and 782.26 eV, which may be attributed to Co^{2+} and Co^{3+}, respectively, in the octahedral positions. XPS shows that d-**Co-F** contains both Co^{2+} and Co^{3+} which may be due to the oxidation of Co^{2+} ions to maintain the charge neutrality of the framework upon removal of the guest from the pores. Thus, XPS analysis confirmed the possible high spin to low spin transition of the metal centre of d-**Co-F** unlike the rest of the MOFs. Considering all these contributions, the overall trend of conductivity among the MOFs after removal of DMA is as follows d-**Mn-F** > d-**Ni-F** > d-**Zn-F** > d-**Co-F**.

From reports it is observed that the grain boundaries significantly affect the conductivity values of conducting materials.[23] To check the inter connectivity between the micro crystalline regions in the pellets, SEM images were taken for one of the pellets (Fig. S10, ESI†). From the SEM images it may be observed that significant gaps are present between the crystalline regions indicating the heterogeneity of the pellet. The heterogeneity in the pellet contributes to grain boundaries which in turn act as barriers to the charge flow.[24,25] As grain boundaries might reduce the charge flow between the microcrystals we can expect that the inherent conductivities of the MOFs to be higher than observed.

Experimental

Materials and methods

All the metal salts used for synthesized were purchased from Sigma-Aldrich and used without further purification. The solvent *N*,*N*-dimethyl formamide (DMF) used was purchased from TCI chemicals. Hydrochloric acid used in the synthesis was purchased from Finar. The FTIR spectra of the compounds were recorded using an Agilent FTIR spectrometer in KBr medium at room temperature in the region 4000–450 cm^{-1}. The surface morphology of the compounds was studied by using a scanning electron microscope (SEM), model No JEOL JSM-6390LV. Thermogravimetric analysis was carried out using a PerkinElmer TGA 4000 V1.04 analyzer, serial number 002042008, over a temperature range of 30–700 °C with a heating rate of 10 °C min^{-1} under a N_2 atmosphere. Powder X-ray diffraction (XRD) data were collected on a Bruker D8 Advance A25 X-ray diffractometer with Cu Kα radiation in the 2θ range from 5° to 80°. Single crystal X-ray diffraction analysis was carried out on a Bruker diffractometer having model number D8Quest.

Conductivity measurement

A Keithley 2400 source meter was used to study *I*–*V* characteristics at room temperature in the frequency range 102–106 Hz. A two-probe technique was used to measure the electrical conductivity of the compounds.

Pellets (1.3 cm diameter, 2 mm thickness) used for conductivity measurements were prepared using a compression-moulding machine with hydraulic pressure *ca.* 2–5 ton. The following equation was used to measure the conductivity,

$$\rho = \frac{V}{I} 2\pi S$$

where ρ is the resistivity of the sample, V is the applied voltage, I is the measured current through the sample, and S is the distance between probes.

Crystallography

The X-ray single crystal diffraction data for all the compounds were collected on a Bruker diffractometer. The data refinement and cell reductions were carried out using a Bruker apex II. The structures were solved by direct methods and refined by full-matrix least-squares calculations using SHELXTL software. All the non-H atoms were refined in the anisotropic approximation against F^2 of all reflections.

Synthetic procedures

Method A. 2 mmol of manganese chloride, 15 mL of DMF (*N*,*N*′-dimethylformamide) and 2 mL of dilute hydrochloric acid were placed in a 50 mL Teflon-lined stainless-steel vessel autoclave. The autoclave was heated at 120 °C for 2 days under autogenous pressure and cooled to room temperature at a cooling rate of 10 °C h^{-1}. Crystals were collected and dried at room temperature overnight.

Method B. Metal salts (cobalt chloride/nickel chloride/zinc chloride) (2 mmol) were dissolved in 8 mL deionized water and 8 mL of DMF (*N*,*N*-dimethylformamide). Then the reaction mixture was transferred into a 50 mL Teflon-lined stainless-steel vessel autoclave. The mixture was heated at 120 °C for three days under autogenous pressure. The resulting solution

was slowly cooled down to room temperature at a cooling rate of 10 °C h^{-1} and then, it was again heated at 90 °C for another two days. The reaction mixture was allowed to cool to room temperature to obtain crystals of the respective MOFs.

Computational details

The structural optimization of all the metal–organic frameworks (MOFs) was carried out using density functional theory (Fig. S12, ESI†). We used the PBE0[26] functional with the combination of the def2TZVP basis set. All the calculations were done by using the Gaussian 16 suite of program.[27] All these structures were found to be at their local minima with real values of the Hessian matrix.

To study the topological features of the optimized structure of MOFs, partial density of states (PDOS) were analyzed using the Multiwfn program of code.[28]

XPS analysis

The XPS data were collected using a Thermo scientific K-Alpha X-ray photoelectron spectrometer equipped with a monochromated, micro-focused, low-power Mg-K_α X-ray source.

Conclusions

In summary we have reported simple and cost-effective synthesis of four highly conductive 3D metal organic frameworks constructed using *in situ* generated ligands. The *in situ* generated formate anion was attributed to the decomposition of the DMF molecules under high pressure and temperature conditions. The decomposition of the DMF molecules also generated dimethyl ammonium cations *in situ* which were entrapped into the pores of MOFs during crystallization which facilitates proton conductivity in the MOFs. Again, the observed conductivity in these four frameworks was also envisaged to be due to the charge flow through the M–O bond of the frameworks. The through bond conductivity and band gaps of the MOFs are governed by the number of unpaired d-electrons and probability of electron exchange between the metal d-orbital and the 2p-orbital of coordinating atoms (oxygen). The band gap and temperature dependent conductivity indicate the semiconducting nature of the MOFs. The removal of the guest molecules from the pores of the MOFs upon heating caused minimum changes in the basic structure of the MOFs as confirmed by PXRD analysis, however, significantly improved the conductivity of MOFs except for the MOF containing the Co^{2+} centre. This improvement in conductivity is thought to be due to the formation of highly mobile hydronium ions and an increase in the number of unpaired d-electrons. Also, a reduction in the lattice vibrations of the M–O bond of the MOFs would have been otherwise contributed by vibrations of guest molecules.

This work highlights the probability of achieving highly conductive MOFs from small ligands which was rarely realized so far. Also, an emphasis is placed on the importance of the development of simple and cost-effective synthetic methods to obtain highly conductive MOFs which otherwise require tedious methods and expensive reagents. This work may also provide deeper insight into structure–property relationships and a new avenue to the development of cost effective and electrically conductive MOFs.

Author contributions

Uddit Narayan Hazarika: investigation, methodology, data curation, visualization and writing – original draft. Jhorna Borah: investigation, methodology, data curation and visualization. Arobinda Kakoti: investigation and data curation. Rinki Brahma: investigation and methodology. Kangkan Sarmah: theoretical investigation and methodology. Ankur Kanti Guha: theoretical investigation, methodology and supervision. Prithiviraj Khakhlary: conceptualization, investigation, methodology, resources, visualization, writing – review and editing and supervision.

Conflicts of interest

There are no conflicts to declare.

Acknowledgements

This work is funded by Science and Engineering Research Board, India (EEQ/2019/000139) and Department of Science and Technology, India (SR/PURSE/2022/142(C)). The authors thank Prof. Jubaraj Bikash Baruah, IIT Guwahati for valuable suggestion and Dr Prasurjya Pitram Mudoi and Dr Surajit Konwer, Department of Chemistry, Dibrugarh University for instrumental help.

Notes and references

1 M. G. Campbell, D. Sheberla, S. F. Liu, T. M. Swager and M. Dinca, *Angew. Chem., Int. Ed.*, 2015, **54**, 4349–4352.
2 S. Zheng, Y. Sun, H. Xue, P. Braunstein, W. Huang and H. Pang, *Natl. Sci. Rev.*, 2022, **9**, 197.
3 S. Bureekaew, S. Horike, M. Higuchi, M. Mizuno, T. Kawamura, D. Tanaka, N. Yanai and S. Kitagawa, *Nat. Mater.*, 2009, **8**, 831–836.
4 L. Sun, C. H. Hendon, M. A. Minier, A. Walsh and M. Dinca, *J. Am. Chem. Soc.*, 2015, **137**, 6164–6167.
5 L. Sun, T. Miyakai, S. Seki and M. Dinca, *J. Am. Chem. Soc.*, 2013, **135**, 8185.
6 M. Hmadeh, Z. Lu, F. Gandara, H. Furukawa, S. Wan, V. Augustyn, R. Chang, L. Liao, F. Zhou, E. Perre, V. Ozolins, K. Suenaga, X. Duan, B. Dunn, Y. Yamamto, O. Terasaki and O. M. Yaghi, *Chem. Mater.*, 2012, **24**, 3511.
7 T. C. Narayan, T. Miyakai, S. Seki and M. Dinca, *J. Am. Chem. Soc.*, 2012, **134**, 12932.
8 Y. Kobayashi, B. Jacobs, M. D. Allendorf and J. R. Long, *Chem. Mater.*, 2010, **22**, 4120.
9 M. Zeng, Q. Wang, Y. Tan, S. Hu, H. Zhao, L. Long and M. Kurmoo, *J. Am. Chem. Soc.*, 2010, **132**, 2561.

10 S. Shang, C. Du, Y. Liu, M. Liu, X. Wang1, W. Gao, Y. Zou, J. Dong, Y. Liu and J. Chen, *Nat. Commun.*, 2022, **13**, 7599.
11 L. S. Xie, G. Skorupskii and M. Dinca, *Chem. Rev.*, 2020, **120**, 8536–8580.
12 Z. Li, L. Du, J. Zhou, L. Li, Y. Hu, Y. Qiao, M. Xie and Q. Zhao, *New J. Chem.*, 2013, **37**, 2473.
13 X. Wang, L. Gan, S. Zhang and S. Gao, *Inorg. Chem.*, 2004, **43**, 4615–4625.
14 R. C. Peralta, R. P. Rodríguez, M. A. L. Ramírez, A. F. Parra, M. Sánchez, I. H. Ahuactzi, L. E. Chiñas, D. J. Ramírez and J. M. Rivera, *J. Mol. Struct.*, 2019, **1189**, 210–218.
15 Y. Wang, R. Cao, W. Bi, X. Li, D. Yuan and D. Sun, *Microporous Mesoporous Mater.*, 2006, **91**, 215–220.
16 Z. Zhu, X. Meng, D. Zhang, X. Zhang, M. Wang, F. Jin and Y. Fan, *J. Solid State Chem.*, 2017, **248**, 109–118.
17 Y. Li, X. Jiang, Z. Fu, Q. Huang, G. E. Wang, W. H. Deng, C. Wang, Z. Li, W. Yin, B. Chen and G. Xu, *Nat. Commun.*, 2020, **11**, 261.
18 Z. Hao, G. Yang, X. Song, M. Zhu, X. Meng, S. Zhao, S. Song and H. Zhang, *J. Mater. Chem. A*, 2014, **2**, 237–244.
19 K. Fan, J. Li, Y. Xu, C. Fu, Y. Chen, C. Zhang, G. Zhang, J. Ma, T. Zhai and C. Wang, *J. Am. Chem. Soc.*, 2023, **145**, 12682–12690.
20 X. LinHua, L. JianBin, L. XiaoMin, X. Wei, Z. WeiXiong, L. ShuXia, Z. JiePeng and C. XiaoMing, *Sci. China: Chem.*, 2010, **53**, 2144–2151.
21 L. Sun, C. H. Hendon, M. A. Minier, A. Walsh and M. Dinca, *J. Am. Chem. Soc.*, 2015, **137**, 6164–6167.
22 Y. Li and R. T. Yang, *Langmuir*, 2007, **23**, 12937–12944.
23 F. Gandara, F. J. Uribe-Romo, D. K. Britt, H. Furukawa, L. Lei, R. Cheng, X. Duan, M. O'Keeffe and O. M. Yaghi, *Chem. – Eur. J.*, 2012, **18**, 10595–10601.
24 R. T. Weitz, K. Amsharov, U. Zschieschang, E. B. Villas, D. K. Goswami, M. Burghard, H. Dosch, M. Jansen, K. Kern and H. Klauk, *J. Am. Chem. Soc.*, 2008, **130**, 4637–4645.
25 I. Vladimirov, M. Kühn, T. Geßner, F. May and R. T. Weitz, *Sci. Rep.*, 2018, **8**, 14868.
26 J. P. Perdew, K. Burke and M. Ernzerhof, *Phys. Rev. Lett.*, 1996, **77**, 3865.
27 M. J. Frisch, G. W. Trucks, H. B. Schlegel, G. E. Scuseria, M. A. Robb, J. R. Cheeseman, G. Scalmani, V. Barone, G. A. Petersson, H. Nakatsuji, X. Li, M. Caricato, A. V. Marenich, J. Bloino, B. G. Janesko, R. Gomperts, B. Mennucci, H. P. Hratchian, J. V. Ortiz, A. F. Izmaylov, J. L. Sonnenberg, D. W. Young, F. Ding, F. Lipparini, F. Egidi, J. Goings, B. Peng, A. Petrone, T. Henderson, J. L. Ranasinghe, V. G. Zakrzewski, J. Gao, N. Rega, G. Zheng, W. Liang, M. Hada, M. Ehara, K. Toyota, R. Fukuda, J. Hasegawa, M. Ishida, T. Nakajima, Y. Honda, O. Kitao, H. Nakai, T. Vreven, K. Throssell, J. A. Montgomery, J. E. Peralta Jr., F. Ogliaro, M. J. Bearpark, J. J. Heyd, E. N. Brothers, K. N. Kudin, V. N. Staroverov, T. A. Keith, R. Kobayashi, J. Normand, K. Raghavachari, A. P. Rendell, J. C. Urant, S. S. Iyengar, J. Tomasi, M. Cossi, J. M. Millam, M. Klene, C. Adamo, R. Cammi, J. W. Ochterski, J. W. Martin, K. Morokuma, O. Farkas, J. B. Foresman and D. J. Fox, *Gaussian*, Gaussian, Inc., Wallingford CT, 2016.
28 R. W. F. Bader, *Atoms in Molecules: A Quantum Theory*, Oxford University Press, Oxford, 1990.